Decline of the Black Sea Oxygen Inventory

Arthur Capet[1,2], Emil V. Stanev[3], Jean-Marie Beckers[4], James W. Murray[5], and
Marilaure Grégoire[2]

[1]OGS, National Institute of Oceanography and Experimental Geophysics, Trieste, Italy
[2]Laboratory of Oceanology, University of Liège, Liège,Belgium
[3]HZG, Helmholtz-Zentrum Geesthacht, Hamburg, Germany
[4]GHER, GeoHydrodynamics and Environment Research, University of Liège, Liège,Belgium
[5]School of Oceanography, University of Washington, Seattle, WA, USA

Correspondence to: A. Capet (arthurcapet@gmail.com)

Abstract.

We show that from 1955 to 2015, the inventory of oxygen in the Black Sea has decreased by 44%
and the basin-averaged oxygen penetration depth has decreased from 140m in 1955 to 90m in 2015,
which is the shallowest annual value recorded during that period.

5   The oxygenated Black Sea surface layer separates the world's largest reservoir of toxic hydrogen
sulphide from the atmosphere. The threat of chemocline excursion events led to hot debates in the
past decades arguing on the vertical stability of the Black Sea oxic/suboxic interface. In the 1970s
and 1980s, when the Black Sea faced severe eutrophication, enhanced respiration rates reduced the
thickness of the oxygenated layer. Re-increasing oxygen inventory in 1985–1995 supported argu-
10   ments in favor of the stability of the oxic layer. Concomitant with a reduction of nutrient loads,
it also supported the perception of a Black Sea recovering from eutrophication. More recently, at-
mospheric warming was shown to reduce the ventilation of the lower oxic layer by lowering Cold
Intermediate Layer (CIL) formation rates.

The debate on the vertical migration of the oxic interface also addressed the natural spatial vari-
15   ability affecting Black Sea properties when expressed in terms of depth. Here we show that using
isopycnal coordinates does not free from a significant spatial variability of oxygen penetration depth.
By considering this spatial variability, the analysis of a composite historical set of oxygen profiles
evidenced a significant shoaling of the oxic layer, and showed that the transient "recovery" of the
1990s was mainly a result of increased CIL formation rates during that period.

20   As both atmospheric warming and eutrophication are expected to increase in the near future,
monitoring the dynamics of the Black Sea oxic layer is urgently required to assess the threat of
further shoaling.

1 Introduction

The Black Sea deep waters constitutes the world's largest reservoir of toxic hydrogen sulphide. 100
meters of ventilated surface waters are all that separate this reservoir from the atmosphere. This
situation results from the permanent halocline (Öszoy and Ünlüata, 1997) that separates the surface
layer (of low salinity due to river inflow) from the deeper layer (of high salinity due to inflowing
Mediterranean seawater), restraining ventilation to the upper layer (Fig. 1).

In the lower part of the halocline, a permanent suboxic layer separates the Black Sea surface
oxygenated waters ($[O_2] > 20\,\mu M$) from the deep sulphidic waters ($[H_2S] > 20\,\mu M$) (Murray et al.,
1989; Tugrul et al., 1992; Murray et al., 1995). More precisely, Murray et al. (1989) considered
a threshold of $10\,\mu M$ of oxygen because they analyzed high quality oxygen data. The threshold of
$20\,\mu M$ of oxygen was applied later to analyze historical oxygen data of lower quality. The upper (O_2
disappearance) and lower (H_2S onset) interfaces of this suboxic layer are controlled by different
biogeochemical and physical processes(Konovalov et al., 2006; Stanev et al., 2014), and undergo
uncorrelated vertical migrations (Konovalov and Murray, 2001). Sinking organic matter is mainly
respirated aerobically within the oxycline, ie. the lower part of the oxygenated layer where oxygen
concentration decreases downwards to $20\,\mu M$. Increasing flux of organic matter, induced by a period
of high nutrient load from the 70s to the late 80s, resulted in higher oxygen consumption above the
suboxic layer and a shoaling of the upper suboxic interface (Codispoti et al., 1991; Konovalov and
Murray, 2001; Tugrul et al., 2014).

After reduction of nutrient inputs around 1990 (Kroiss et al., 2006), the Black Sea was described
as a recovering ecosystem (Mee et al., 2005; Oguz et al., 2006). This perspective was supported by
improved eutrophication indices in the open sea (Kideys, 2002) as well as the stabilization of the
upper suboxic interface in the 90s (Konovalov and Murray, 2001). However, the time scale of the
expected recovery, ie. the time scale associated with the chain of biogeochemical mechanisms re-
lating oxycline penetration depth to riverine nutrient loads, is not quantitatively understood. Several
processes cause the oxycline depth to respond with a time lag to the reduction of riverine nutrient
inputs. First, nutrients are mainly delivered to the northwestern shelf, where the accumulation of
organic matter in the sediments buffers the riverine inputs, with slow diagenetic processes control-
ling and delaying the nutrient outflow across the seaward boundary (Capet et al., 2013). Second,
the intermediate oxidation–reduction cycling of nitrogen, sulfur, manganese, iron and phosphorus
that separates oxygen from hydrogen sulphide (Shaffer, 1986; Codispoti et al., 1991; Konovalov
et al., 2006; Yakushev et al., 2007) can delay the response of the lower suboxic interface to changing
nutrient fluxes by several years (Konovalov et al., 2006).

In addition to these biogeochemical factors, the dynamics of the upper and lower interfaces of the
suboxic layer are controlled by physical processes (Konovalov et al., 2006; Stanev et al., 2014). In
the Black Sea, dense waters formed by winter cooling and mixing Staneva and Stanev (2002) do
not sink to the deepest layer, as in the Mediterranean sea, but accumulate on top of the permanent

2

halocline (Fig. 1). The resulting Cold Intermediate Layer (CIL) is a major feature of the Black Sea vertical structure. Cold intermediate water formation and advection by the cyclonic basin-wide Rim Current (Öszoy and Ünlüata, 1997; Capet et al., 2012) ventilate the oxycline and thereby influence variability in the depth of the upper suboxic interface (Konovalov et al., 2006). Recently, atmospheric warming (Oguz et al., 2006) was shown to reduce the ventilation of the lower oxic layer (Tugrul et al., 2014; Pakhomova et al., 2014). At deeper levels, the dense sinking plume formed by the Mediterranean inflow through the Bosporus, which entrains water from the overlying CIL, injects fingers of oxygenated water directly into the deeper part of the suboxic layer and upper sulphidic layer and thus acts to control the depth of the lower suboxic interface (Konovalov and Murray, 2001; Konovalov et al., 2003; Glazer et al., 2006; Konovalov et al., 2006).

Previous long–term analyses of the vertical migration of the suboxic interfaces either ended (1955–1995 (Konovalov and Murray, 2001)) or started (1985–2015 (Pakhomova et al., 2014)) with the eutrophication period, excluding the large–scale overview required to grasp the interactions of eutrophication and climate factors. Those analyses lacked a comprehensive consideration of the natural spatial and seasonal variability of the vertical distribution of oxygen.

In the presence of large gradients, uneven data distribution may induce artificial signals when inter–annual trends are assessed from direct annual averages. In the stratified Black Sea, properties expressed in terms of depth coordinates (m) present a high spatial variability due to mesoscale features (Kempe et al., 1990) and to the general curvature of Black Sea isopycnals (Öszoy and Ünlüata, 1997; Stanev et al., 2014). As an alternative, using density (isopycnal levels, σ_θ) as vertical coordinate is generally considered a stable solution to assess the vertical migration of the chemocline on a decadal scale (Tugrul et al., 1992; Saydam et al., 1993; Murray et al., 1995). However, the spatial confinement of the lateral oxygen injections associated with the Bosporus plume, as well as the spatial variability of diapycnal ventilating processes (Zatsepin et al., 2007), imposes an horizontal structure to the oxygen penetration depth when expressed in terms of density (Stanev et al., 2004; Glazer et al., 2006). As this spatial gradient might scale with the temporal variations (a range of 0.17 $\mathrm{kg\,m^{-3}}$ was observed during the Knorr2003 campaign, Glazer et al. (2006)), it has to be considered when deriving interannual trends.

The present study describes the application of the DIVA (Data-Interpolating Variational Analysis) detrending procedure (Troupin et al., 2012; Capet et al., 2014) to untangle the temporal and spatial variability of three indices related to the Black Sea oxygenation status: the depth and density level of oxygen penetration and the oxygen inventory. These values were diagnosed from a composite historical dataset of oxygen vertical profiles. We reviewed the evolution of those indices through the past 60 years and discuss the respective controls of eutrophication and climate factors.

2 Material and methods

2.1 Data

We gathered a composite set of 4385 ship-based vertical profiles (oxygen, temperature and salinity) obtained between 1955 and 2005 in the Black Sea using CTD rosette bottles, continuous pumping profilers (Codispoti et al., 1991) and in situ analyzers (Glazer et al., 2006) from the World Ocean Database (http://www.nodc.noaa.gov/OC5/SELECT/dbsearch/dbsearch.html), R/V Knorr 2003 and R/V Endeavor 2005 campaigns (http://www.ocean.washington.edu/cruises/Knorr2003/,http://www.ocean.washington.edu/cruises/Endeavor2005/). Only the profiles containing at least 5 observation depths, one observation above 30 m depth and one record with $[O_2] < 20$ μM were retained for analysis. The temporal and spatial distribution of the selected ship-based profiles are displayed in Figs. 2 and 3, respectively.

To complement the analysis of ship-based casts, we considered profiles originating from ten Argo autonomous profilers (May 2010–December 2015). Only good quality-checked real-time data were considered (Carval et al., 2014). Two of these floats (Argo ID 7900465 and 7900466) have been presented and discussed by Stanev et al. (2013), where the consistence and comparability of Argo and historical profiles is asserted within a 1μM error range.

Several studies address the error of Argo real-time oxygen data (e.g., Bittig and Körtzinger, 2015; Takeshita et al., 2013; Johnson et al., 2015). Demonstrating that the Black Sea real-time Argo data are precisely (ie, at fine scales) comparable with historical Winkler data, or identifying the relevant correction, is beyond the scope of the present study which addresses monthly to decadal time scales. Evenly distributed small scales error (eg., difference between ascending and descending profiles due to sensor time response) were thus filtered by the temporal smoothing. However, a systematic error is not strictly excluded which could reach an underestimation of 10 μM (Virginie Thierry, IFREMER, personal communication, January 2016). Therefore, we evaluated a "worst-case" scenario in the analysis of Argo data by considering a systematic underestimation of oxygen concentration by 10μM.

Although most of the floats drifted along the basin periphery, some were also advected in the central part (Fig. 3). These trajectories highlight the range of spatial variability for the diagnostics described in Sect. 2.2.

The investigation time frame was divided into periods according to data availability and to dissociate known phases of eutrophication (Oguz, 2008; Kroiss et al., 2006) and CIL dynamics (Piotukh et al., 2011; Capet et al., 2014) (see also Oguz et al. (2006) for decadal cycles in the Black Sea): 1955–1975 (1575 ship-based profiles), 1976–1985 (1350 ship-based profiles), 1986–1998 (1324 ship-based profiles) and 1999–2015 (136 ship-based profiles and 1393 Argo profiles).

2.2 Profile analysis

From each profile we derived (1) the depth and (2) the potential density anomaly σ_θ where oxygen concentration went below 20 μM and (3) the oxygen inventory, integrated above this limit (Fig. 1). The threshold value of 20 μM used to define the upper interface of the suboxic layer was suggested to compare oxygen observations issued from sensors with different detection limits (Konovalov and Murray, 2001). To evaluate how a 10 μM underestimation by Argo profilers would affect the main conclusions, oxygen penetration depths an density levels for Argo were also computed using a threshold of 10 μM.

The CIL cold content (Fig. 1) was diagnosed from corresponding salinity and temperature profiles following Capet et al. (2014). It indicates on the intensity of CIL formation smoothed over 4-5 years, i.e. the residence time of cold intermediate waters (Staneva and Stanev, 2002; Piotukh et al., 2011; Capet et al., 2014).

$$\text{CIL cold content} = c\rho \int\limits_{\text{CIL}} [T(z) - T_{CIL}] dz, \tag{1}$$

where ρ is the density and c the heat capacity and $T_{CIL} = 8.35\,^\circ\text{C}$ (Stanev et al., 2013).

2.3 DIVA analysis

Climatologies for the whole period and interannual trends were identified for the three oxygen diagnostics by applying the DIVA detrending algorithm on the ship-based data set (see details in Appendix A).

In short, the DIVA interpolation software (http://modb.oce.ulg.ac.be/mediawiki/index.php/DIVA Troupin et al. (2012)) computes a gridded climatology obtained by minimizing a cost function which penalize gradients and misfits with observations. The DIVA detrending algorithm (Capet et al., 2014) computes trends for each year, i.e. the average difference between data pertaining to this year and the spatial analysis at these data locations. This procedure allows one to account for the sampling error associated with spatial/temporal variability.

3 Results

3.1 Spatial variability

The spatial distribution of the oxygen penetration depth (Fig. 4a) reflects the general curvature of the Black Sea vertical structure. A range of approximately 70 m was observed between oxygen penetration depth in the periphery (150 m) and in the central part (80 m).

A significant spatial variability remains when expressing oxygen penetration in terms of potential density anomaly, σ_θ, (Fig. 4b). While the central part bears typical values of 15.75 $\text{kg}\,\text{m}^{-3}$, a deeper anomaly (in terms of density) can be seen in the area of the Bosporus plume (16.1 $\text{kg}\,\text{m}^{-3}$), which

then decreases along the southern (15.85-15.9 $\mathrm{kg\,m^{-3}}$) and eastern periphery (15.85 $\mathrm{kg\,m^{-3}}$). These result in a range of spatial variability of 0.35 $\mathrm{kg\,m^{-3}}$.

The spatial distribution of the oxygen inventory (Fig. 4c) follows that of the oxygen penetration depth. The range of spatial variability reaches 12 $\mathrm{mol\,O\,m^{-2}}$, ie. between 17 $\mathrm{mol\,O\,m^{-2}}$ in the central part and 29 $\mathrm{mol\,O\,m^{-2}}$ in the periphery.

The ranges of spatial variability derived from theses spatial analysis agreed with those depicted by the Argo profilers (Fig. 5), bearing in mind the different time scales under consideration.

3.2 Temporal variability

Between 1955-2005, the oxygen penetration depth rose by an average rate of 7.9 m per decade (Fig. 6a). The basin average was of 140 m in 1955 (ship-based), 100 m in 2005 (ship-based) and 90 m in 2015 (Argo). Considering a systematic underestimation by 10 μM in the Argo data would result in an oxygen penetration depth around 95 m for 2015 (Argo).

This shoaling was also observed on the potential density scale (-0.074 $\mathrm{kg\,m^{-3}}$ per decade, Fig. 6b). The basin average was of 16.05 $\mathrm{kg\,m^{-3}}$ in 1955 (ship-based), 15.6 $\mathrm{kg\,m^{-3}}$ in 2005 (ship-based) and around 15.3 $\mathrm{kg\,m^{-3}}$ in 2015 (Argo). Considering a systematic underestimation by 10 μM in the Argo data would result in values of 15.5 m for 2015 (Argo).

The oxygen inventory, integrated from the surface down to the suboxic upper interface, decreased by 44% during the last 60 years (Fig. 6c), considering the ship-based estimate for 1955 (27 $\mathrm{mol\,O\,m^{-2}}$) and the Argo estimate for 2015 (15 $\mathrm{mol\,O\,m^{-2}}$). The few ship-based profiles available after the mid 90s revealed the lowest oxygen inventories recorded during the time frame covered by the present study.

The temporal signals departed from these linear trends between 1988 and 1996, during which deeper oxygen penetration (both in terms of depth and density) and higher oxygen content were observed.

3.3 Oxygen inventory and CIL cold content

Positive relationships between oxygen inventory and CIL cold content were obtained for all periods (Fig. 7). Considering a given level of CIL cold content, the corresponding oxygen inventory decreased significantly from period 1955–1975 to period 1986–1998 (Fig. 7b).

The relationship between oxygen inventory and CIL cold content for the period 1999–2015 does not differ significantly from that obtained for the period 1986–1998 (Fig. 7b). This comparison should be considered with caution, however, as oxygen profiles for the period 1999–2015 originate mainly from Argo floats whose sampling rate is much higher than ship-based casts.

High CIL cold content are much more frequent during the period 1986–1998, while low CIL cold content are more frequent during 1999-2013.

4 Discussion

195 The spatial analysis of oxygen penetration depth showed that the use of density coordinates does not eliminate the sampling error associated with uneven spatial coverage (Fig. 4). Deeper pycnal oxygen penetration in the Bosporus area were expected, in relation with the intermediate lateral injections associated with the Bosporus plume. In addition, deeper pycnal oxygen penetration in the southern and eastern periphery suggests the occurrence of diapycnal ventilation along the steep bathymetry

200 (Zatsepin et al., 2007). The aggregation of the most recent ship-based profiles in the Bosporus area and in the southeastern region (Fig. 3), might have led to an overestimation of the basin-average oxygen penetration depth in the last decade, hence to an underestimation of the shoaling trend of the Black Sea oxic layer.

 Considering spatial variability revealed a clear shoaling trend for oxygen penetration depth. This

205 shoaling can be seen on both depth and density scales (Fig. 6a,b). This confirms the hypothesis that the shoaling of oxygen penetration depth is not due to a general shoaling of the main halocline, but is associated with a shifted biogeochemical balance in the oxygen budget (Codispoti et al., 1991; Konovalov and Murray, 2001; Tugrul et al., 2014).

 Using σ_θ coordinates depicts clearer temporal variations (Fig. 5 and Fig. 6). The shoaling rate

210 varies in time and was more intense during 1970–1985 and from 1996 onwards. Argo diagnostics using different oxygen threshold show a larger discrepancy in the case of pycnal coordinates. The co-occurrence of density and oxygen gradients (Fig. **??**) results in a higher sensitivity to the sensor accuracy for the σ_θ diagnostic for oxygen penetration. However, even a systematic underestimation by 10 μM of oxygen concentration by Argo profilers does not invalidate our results.

215 The positive correlations between CIL cold content and oxygen inventory observed for all the periods illustrate the ventilation of intermediate layers by CIL formation and advection (Fig. 7b). In the early 90s, the transient recovery of the three oxygenation diagnostics (Figs. 6a, b, c, 7a) provided arguments supporting the stability of the oxic interface (Tugrul et al., 1992; Buesseler et al., 1994). This stabilization matched the convenient perception of a general recovery of the Black

220 Sea ecosystem after the reduction of nutrient load around 1990 (Kroiss et al., 2006). However, Fig. 7 indicates that the oxygenation diagnostics obtained for the period 1986–1998 were associated with much higher ventilation rates (ie, higher CIL cold content) than during the previous periods. If, in response to nutrient reduction, the biogeochemical oxygen consumption terms had been lower during the period 1986–1998 than previously, the increased ventilation during that period would

225 have resulted in higher oxygen inventories. Instead, oxygen inventories observed during 1986–1998 are lower than those observed in the previous decade for similar levels of CIL cold content. We conclude that high CIL formation rates during this period (Piotukh et al., 2011; Capet et al., 2014) provided enough ventilation to mask ongoing high oxygen consumption.

 The fact that the relationship between oxygen inventories and CIL content for the last period

230 1999-2015 is similar to that of 1986–1998 indicates a stabilization in the biogeochemical oxygen

consumption terms. Higher air temperature in this last period (Oguz and Cokacar, 2003; Oguz et al., 2006; Pakhomova et al., 2014), by limiting winter convective ventilation events (Capet et al., 2014) led to the lower oxygen inventories ever recorded for the Black Sea (Fig. 6c).

Fore-casted global warming, without excluding transient high ventilation periods, will limit CIL water formation(Capet et al., 2014) and reduce the oxygenation of the Black Sea intermediate layers. At the same time, uncertainties remain regarding the capacity of re-flourishing economies of the lower Danube watershed to recover their productivity in a more sustainable, less polluting form. Economic development in the Danube Basin could reverse the improving situation of eutrophication if nutrients are not managed properly (Kroiss et al., 2006). Under these conditions, there is no reason to expect that the oxycline shoaling observed over the past 60 years will stabilize.

There are reasons to worry about a rising oxycline in the Black Sea. First, biological activity is distributed vertically on the whole oxygenated layer, as indicated by zooplankton dial migration Ostrovskii and Zatsepin (2011). The reduction of the oxygenated volume described in this study could therefore have impacted on Black Sea living stocks by reducing carrying capacity and increasing predation encounter rates. It would come in timely to estimate now the impact that a further shoaling of the oxic interfaces would bear on the Black Sea resources for the fishing industry.

Second, under present conditions, a massive atmospheric release of hydrogen sulphide caused by a sudden outcropping of anoxic waters remains unlikely, due to the stability of the Black Sea pycnal structure. Such outcropping event of sulphidic waters would have dramatic ecological and economical consequences(Mee, 1992). On the 27th October 2005, an anomalous quasi-tropical cyclone was observed over the western Black Sea that led, in a few days, to the outcropping of waters initially located at 30 m depth (Efimov et al., 2008). Two years earlier, sulphide was measured in the same area (western central gyre) around 80 m (Glazer et al., 2006). Because global warming is expected to increase the occurrence of extreme meteorological events (Beniston et al., 2007), every meter of oxycline shoaling would bring the Black Sea chemocline excursion events closer to the realm of possibility.

5 Conclusions

The present study evidenced the decline of the Black Sea oxygen inventory during the second half of the XXth century and first decade of XXIth and highlighted the threat that further atmospheric warming casts upon the vertical stability of the Black Sea oxygenated layer.

Further works are urgently required to assess how actual nutrient emission policies adequately prevents, in the context of fore-casted warming, the ecological and economical damages that would arise from a further shoaling of the oxic interface.

Spatially-resolved biogeochemical models are needed to integrate explicitly the interacting processes affecting the Black Sea oxycline. here.

It is also essential (1) to determine to which extent the shoaling of the oxygen penetration depth entrains a shoaling of the the sulphidic onset depth; (2) to set up a continuous monitoring of the Black Sea oxygen inventory and the intensity of winter convective ventilation (through CIL cold content); and (3) to clarify and quantify the interplays of diapycnal and isopycnal ventilation mechanisms and, in particular, the role played by the peripheral permanent/semi-permanent mesoscale structures and how this relates to the intensity of the Rim Current (Stanev et al., 2014; Kubryakov and Stanichny, 2015). We propose that these objectives might be answered by maintaining in the Black Sea a minimum population of both moored and drifting autonomous profilers equipped with oxygen and sulphidic sensors.

Appendix A: The DIVA detrending algorithm

DIVA (Data-Interpolating Variational Analysis) is a method for spatial interpolation. Its principle is to construct an analyzed field φ that satisfies a set of constraints expressed in the form of a cost function over a spatial domain Ω. The cost function is made up of (1) an *observation constraint*, which penalizes the misfit between data and analysis, and (2) a *smoothness constraint*, which penalizes the irregularity of the analyzed field (gradients, Laplacian etc).

Let us assume that we work with data anomalies, i.e. a reference (or background) field is subtracted from the data points prior the analysis. For N data anomalies d_i at locations (x_i, y_i), the cost function reads, in Cartesian coordinates:

$$
\begin{aligned}
J[\varphi] \quad = \quad & \int_{\Omega} \left(\boldsymbol{\nabla}\boldsymbol{\nabla}\varphi : \boldsymbol{\nabla}\boldsymbol{\nabla}\varphi + \alpha_1 \boldsymbol{\nabla}\varphi \cdot \boldsymbol{\nabla}\varphi + \alpha_0 \varphi^2 \right) \mathrm{d}\Omega \quad\quad\quad\quad\quad (A1) \\
& + \sum_{i=1}^{N} \mu_i \left[d_i - \varphi(x_i, y_i) \right]^2 = J_{\mathrm{smooth}}[\varphi] + J_{\mathrm{obs}}[\varphi],
\end{aligned}
$$

where μ_i, α_0 and α_1 are coefficients related to characteristics of the dataset. $\boldsymbol{\nabla}$ is the horizontal gradient operator and $\boldsymbol{\nabla}\boldsymbol{\nabla}\varphi : \boldsymbol{\nabla}\boldsymbol{\nabla}\varphi = \sum_i \sum_j (\partial^2\varphi/\partial x_i \partial x_j)(\partial^2\varphi/\partial x_i \partial x_j)$, the generalization of the scalar product of two vectors.

The first term of (A1) measures the spatial variability (curvature, gradient and value) of the analyzed field and is identified as the smoothness constraint. The second term is a weighted sum of data-analysis misfits and is identified as the observation constraint: it tends to pull the analyzed field towards the observations. The coefficients of (A1) can be determined from: (1) the relative weights w_i attributed to each observation d_i, (2) the correlation length L and (3) the signal-to-noise ratio λ (Troupin et al., 2012). The analyses presented in this study were achieved with equal weights $w_i = 1$, $L = 0.8°$ and $\lambda = 0.5$. The minimization of A1 is solved over Ω with a finite-element technique (Brasseur et al., 1996) which excludes data influence across land points Troupin et al. (2010).

The detrending algorithm, presented in (Capet et al., 2014) with synthetic and real case studies, proceeds as follows. Input data can be classified amongst the different classes C_j (e.g. 1990, 1991,

...) of a given group C (e.g. the year). The observation constraint of the functional (A1) can then be rewritten by including an unknown trend value for each class $(d_{C_1}, d_{C_2}, \ldots)$:

$$
\begin{aligned}
J_{\mathrm{obs}}[\varphi] &= \sum_{i \in C_1} \mu_i \left[d_i - d_{C_1} - \varphi(x_i, y_i) \right]^2 \\
&+ \sum_{i \in C_2} \mu_i \left[d_i - d_{C_2} - \varphi(x_i, y_i) \right]^2 + \ldots
\end{aligned} \tag{A2}
$$

If the function $\varphi(x, y)$ were known, minimization with respect to each of the unknowns d_{C_j} would yield

$$
d_{C_1} = \frac{\sum_{i \in C_1} \mu_i \left[d_i - \varphi(x_i, y_i) \right]}{\sum_{i \in C_1} \mu_i} \tag{A3}
$$

and similarly for the other classes: the trend for each class is the weighted misfit of the class with respect to the overall analysis.

Using an analysis without detrending as a first guess for φ, trends are computed for each classes in each group and subtracted from the original data. Following this, a new analysis is performed, the trends are recalculated, and the iterations continue until a specified convergence criterion is fulfilled. The procedure can be generalized with several groups of classes. The present study considered years and months.

The DIVA software and up-to-date related informations can be found on
http://modb.oce.ulg.ac.be/mediawiki/index.php/DIVA.

References

Beniston, M., Stephenson, D. B., Christensen, O. B., Ferro, C. A., Frei, C., Goyette, S., Halsnaes, K., Holt,
325   T., Jylhä, K., Koffi, B., et al.: Future extreme events in European climate: an exploration of regional climate
model projections, Climatic Change, 81, 71–95, 2007.

Bittig, H. C. and Körtzinger, A.: Tackling oxygen optode drift: Near-surface and in-air oxygen optode measure-
ments on a float provide an accurate in-situ reference, Journal of Atmospheric and Oceanic Technology, p.
150310071431006, 2015.

330   Brasseur, P., Beckers, J.-M., Brankart, J.-M., and Schoenauen, R.: Seasonal temperature and salinity fields in
the Mediterranean Sea: Climatological analyses of a historical data set, Deep-Sea Research Part I : Oceano-
graphic Research Papers, 43, 159–192, doi:10.1016/0967-0637(96)00012-X, 1996.

Buesseler, K., Livingston, H., Ivanov, L., and Romanov, A.: Stability of the oxic-anoxic interface in the Black
Sea, Deep-Sea Research Part I : Oceanographic Research Papers, 41, 283–296, 1994.

335   Capet, A., Barth, A., Beckers, J.-M., and Grégoire, M.: Interannual variability of Black Sea's hydrodynam-
ics and connection to atmospheric patterns, Deep-Sea Research Part II : Topical Studies in Oceanog-
raphy, 77-80, 128–142, doi:10.1016/j.dsr2.2012.04.010, http://www.sciencedirect.com/science/article/pii/
S0967064512000586, satellite Oceanography and Climate Change, 2012.

Capet, A., Beckers, J.-M., and Grégoire, M.: Drivers, mechanisms and long-term variability of seasonal hypoxia
340   on the Black Sea northwestern shelf — is there any recovery after eutrophication?, Biogeoscience, 10, 3943–
3962, 2013.

Capet, A., Troupin, C., Carstensen, J., Grégoire, M., and Beckers, J.-M.: Untangling spatial and temporal trends
in the variability of the Black Sea Cold Intermediate Layer and mixed Layer Depth using the DIVA detrend-
ing procedure, Ocean Dynamics, 64, 315–324, 2014.

345   Carval, T., Keeley, B., Takatsuki, Y., Yoshida, T., Stephen, L., Schmid, C., Goldsmith, R., Wong, A., McCreadie,
R., Thresher, A., and Tran, A.: Argo User's manual, 2014.

Cleveland, W. S., Grosse, E., and Shyu, W. M.: Local regression models, in: Statistical models in S, edited by
Chambers, J. and Hastie, T., Wadsworth & Brooks/Cole, 1992.

Codispoti, L., Friederich, G., Murray, J., and Sakamoto, C.: Chemical variability in the Black Sea: implica-
350   tions of continuous vertical profiles that penetrated the oxic/anoxic interface, Deep-Sea Research Part I :
Oceanographic Research Papers, 38, S691–S710, 1991.

Efimov, V., Stanichnyi, S., Shokurov, M., and Yarovaya, D.: Observations of a quasi-tropical cyclone over the
Black Sea, Russian Meteorology and Hydrology, 33, 233–239, 2008.

Glazer, B. T., Luther, G. W., Konovalov, S. K., Friederich, G. E., Trouwborst, R. E., and Romanov, A. S.:
355   Spatial and temporal variability of the Black Sea suboxic zone, Deep-Sea Research Part II : Topical Studies
in Oceanography, 53, 1756–1768, 2006.

Johnson, K. S., Plant, J. N., Riser, S. C., and Gilbert, D.: Air Oxygen Calibration of Oxygen Optodes on a
Profiling Float Array, Journal of Atmospheric and Oceanic Technology, 32, 2160–2172, 2015.

Kempe, S., Liebezett, G., and Diercks, A.-R.: Water balance in the Black Sea, Nature, 346, 419, 1990.

360   Kideys, A. E.: Fall and rise of the Black Sea ecosystem, Science, 297, 1482–1484, 2002.

Konovalov, S., Murray, J. W., Luther, G., and Tebo, B.: Processes controlling the redox budget for
the oxic/anoxic water column of the Black Sea, Deep-Sea Research Part II : Topical Studies

in Oceanography, 53, 1817–1841, doi:10.1016/j.dsr2.2006.03.013, http://www.sciencedirect.com/science/article/B6VGC-4KSSW7D-1/2/f04cc2994d928a16eacb1af3868b9b08, Black Sea Oceanography, 2006.

365 Konovalov, S. K. and Murray, J. W.: Variations in the chemistry of the Black Sea on a time scale of decades (1960–1995), Journal of Marine Systems, 31, 217–243, http://www.sciencedirect.com/science/article/pii/S0924796301000549, 2001.

Konovalov, S. K., Luther III, G., Friederich, G. E., Nuzzio, D. B., Tebo, B. M., Murray, J. W., Oguz, T., Glazer, B., Trouwborst, R. E., Clement, B., et al.: Lateral injection of oxygen with the Bosporus plume—fingers of

370 oxidizing potential in the Black Sea, Limnology and Oceanography, 48, 2369–2376, 2003.

Kroiss, H., Zessner, M., and Lampert, C.: daNUbs: lessons learned for nutrient management in the Danube Basin and its relation to Black Sea euthrophication, Chemistry and Ecology, 22, 347–357, 2006.

Kubryakov, A. and Stanichny, S.: Seasonal and interannual variability of the Black Sea eddies and its dependence on characteristics of the large-scale circulation, Deep-Sea Research Part I : Oceanographic Research

375 Papers, 97, 80–91, 2015.

Mee, L., Friedrich, J., and Gomoiu, M.-T.: Restoring the Black Sea in times of uncertainty., Oceanography, 18, 32–43, 2005.

Mee, L. D.: The Black Sea in crisis: a need for concerted international action., Ambio, 21, 278–86, 1992.

Murray, J., Jannasch, H., Honjo, S., Anderson, R., Reeburgh, W., Top, Z., Friederich, G., Codispoti, L., and

380 Izdar, E.: Unexpected changes in the oxic/anoxic interface in the Black Sea, Nature, 338, 411–413, 1989.

Murray, J. W., Codispoti, L. A., and Friederich, G. E.: Oxidation/reduction environments, Aquatic Chemistry, pp. 157–176, 1995.

Oguz, T., ed.: State of the Environment of the Black Sea (2001 - 2006/7), Publications of the Commission on the Protection of the Black Sea Against Pollution (BSC), http://www.blacksea-commission.org/_publ-SOE2009.

385 asp, 2008.

Oguz, T. and Cokacar, T.: Climatic warming and accompanying changes in the ecological regime of the Black Sea during 1990s, Global Biogeochemichal Cycles, 17, doi:10.1029/2003GB002031, 2003.

Oguz, T., Dippner, J. W., and Kaymaz, Z.: Climatic regulation of the Black Sea hydro-meteorological and ecological properties at interannual-to-decadal time scales, Journal of Marine Systems, 60, 235–254,

390 doi:10.1016/j.jmarsys.2005.11.011, http://www.sciencedirect.com/science/article/pii/S092479630500206X, 2006.

Ostrovskii, A. and Zatsepin, A.: Short-term hydrophysical and biological variability over the northeastern Black Sea continental slope as inferred from multiparametric tethered profiler surveys, Ocean Dynamics, 61, 797–806, 2011.

395 Öszoy, E. and Ünlüata, Ü.: Oceanography of the Black Sea: a review of some recent results., Earth-Science Reviews, 42, 231–272, 1997.

Pakhomova, S., Vinogradova, E., Yakushev, E., Zatsepin, A., Shtereva, G., Chasovnikov, V., and Podymov, O.: Interannual variability of the Black Sea Proper oxygen and nutrients regime: The role of climatic and anthropogenic forcing, Estuarine, Coastal and Shelf Science, 140, 134–145, 2014.

400 Piotukh, V., Zatsepin, A. G., Kazmin, A., and Yakubenko, V.: Impact of the Winter Cooling on the Variability of the Thermohaline Characteristics of the Active Layer in the Black Sea, Oceanology, 51, 221–230, 2011.

Saydam, C., Tugrul, S., Basturk, O., and Oguz, T.: Identification of the oxic/anoxic interface by isopycnal surfaces in the Black Sea, Deep-Sea Research Part I : Oceanographic Research Papers, 40, 1405–1412, 1993.

405 Shaffer, G.: Phosphate pumps and shuttles in the Black Sea, Nature, 321, 515–517, 1986.

Stanev, E., Staneva, J., Bullister, J., and Murray, J. W.: Ventilation of the Black Sea pycno-cline. Parameterization of convection, numerical simulations and validations against observed chlo-rofluorocarbon data, Deep-Sea Research Part I : Oceanographic Research Papers, 51, 2137–2169, doi:10.1016/j.dsr.2004.07.018, http://www.sciencedirect.com/science/article/B6VGB-4DN17DM-1/410 2/c889c55405c12a02e8d7c3e725814eef, 2004.

Stanev, E., He, Y., Grayek, S., and Boetius, A.: Oxygen dynamics in the Black Sea as seen by Argo profiling floats, Geophysical Research Letters, 2013.

Stanev, E. V., He, Y., Staneva, J., and Yakushev, E.: Mixing in the Black Sea detected from the temporal and spatial variability of oxygen and sulfide – Argo float observations and numerical modelling, Biogeosciences, 415 11, 5707–5732, doi:10.5194/bg-11-5707-2014, http://www.biogeosciences.net/11/5707/2014, 2014.

Staneva, J. and Stanev, E.: Water mass formation in the Black Sea during 1991–1995, Journal of Marine Sys-tems, 32, 199–218, doi:10.1016/S0924-7963(02)00038-6, http://www.sciencedirect.com/science/article/pii/S0924796302000386, 2002.

Takeshita, Y., Martz, T. R., Johnson, K. S., Plant, J. N., Gilbert, D., Riser, S. C., Neill, C., and Tilbrook, B.: 420 A climatology-based quality control procedure for profiling float oxygen data, Journal of Geophysical Re-search: Oceans, 118, 5640–5650, 2013.

Troupin, C., Machín, F., Ouberdous, M., Sirjacobs, D., Barth, A., and Beckers, J.-M.: High-resolution cli-matology of the North-East Atlantic using Data-Interpolating Variational Analysis (DIVA), Journal of Geophysical Research, 115, C08 005, doi:10.1029/2009JC005512, http://www.agu.org/pubs/crossref/2010/425 2009JC005512.shtml, 2010.

Troupin, C., Sirjacobs, D., Rixen, M., Brasseur, P., Brankart, J.-M., Barth, A., Alvera-Azcárate, A., Capet, A., Ouberdous, M., Lenartz, F., Toussaint, M.-E., and Beckers, J.-M.: Generation of analysis and consistent error fields using the Data Interpolating Variational Analysis (DIVA), Ocean Modelling, 52-53, 90–101, doi:10.1016/j.ocemod.2012.05.002, http://www.sciencedirect.com/science/article/pii/S1463500312000790, 430 2012.

Tugrul, S., Basturk, O., Saydam, C., and Yilmaz, A.: Changes in the hydrochemistry of the Black Sea inferred from water density profiles, Nature, 359, 137–139, 1992.

Tugrul, S., Murray, J. W., Friederich, G. E., and Salihoğlu, İ.: Spatial and temporal variability in the chemical properties of the oxic and suboxic layers of the Black Sea, Journal of Marine Systems, 135, 29–43, 2014.

435 Yakushev, E., Pollehne, F., Jost, G., Kuznetsov, I., Schneider, B., and Umlauf, L.: Analysis of the water column oxic/anoxic interface in the Black and Baltic seas with a numerical model, Marine Chemistry, 107, 388–410, 2007.

Zatsepin, A., Golenko, N., Korzh, A., Kremenetskii, V., Paka, V., Poyarkov, S., and Stunzhas, P.: Influence of the dynamics of currents on the hydrophysical structure of the waters and the vertical exchange in the active 440 layer of the Black Sea, Oceanology, 47, 301–312, 2007.
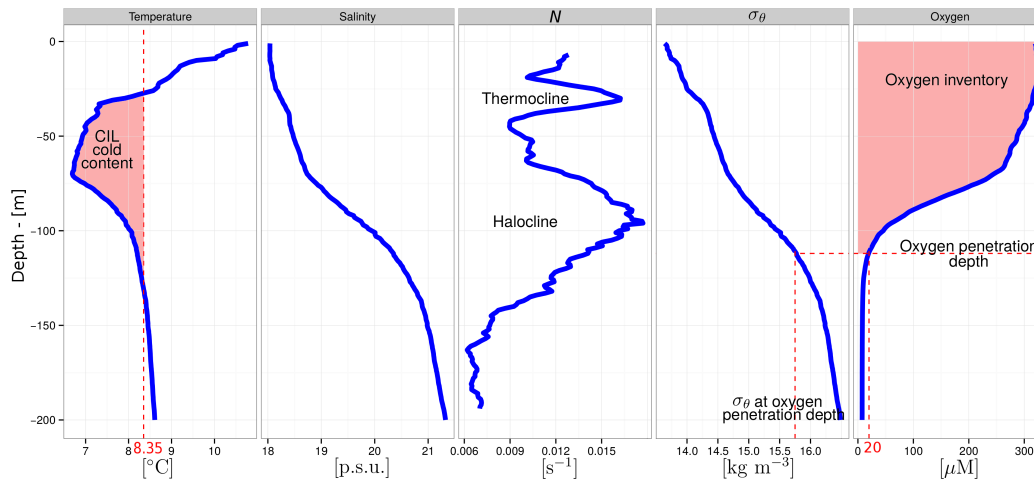
Figure 1. Typical profiles of temperature, salinity, Brunt-Väisälä frequency (N), potential density anomaly (σ_θ) and oxygen concentration in the central Black Sea (May). Note the two peaks in the vertical stratification: the thermocline, which is seasonal and corresponds roughly to the upper limit of the Cold Intermediate layer and the halocline, which is permanent, and correspond roughly to the lower limit of the Cold Intermediate layer and the upper boundary of the suboxic zone. Red dotted lines and shaded areas illustrate the diagnostic values derived from each profiles (Sect. 2.2).
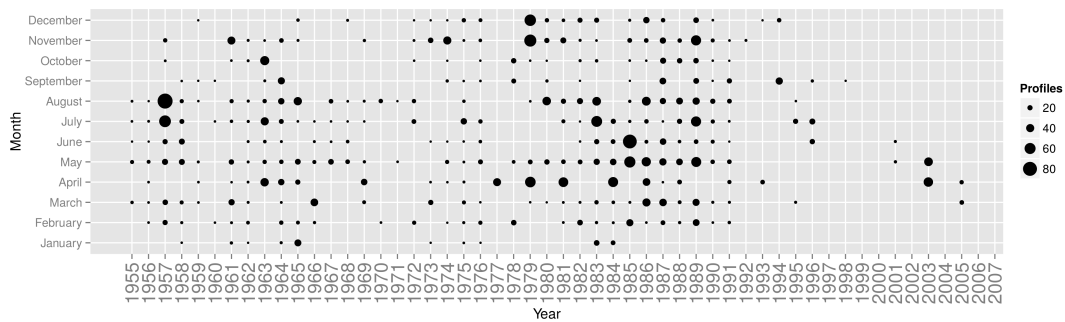
Figure 2. Temporal distribution of the ship-based oxygen profiles merged from the World Ocean Database, R/V Knorr 2003 and R/V Endeavor 2005 campaigns. Only the profiles containing at least 5 observation depths, one observation above 30 m depth and one record with $[O_2] < 20\ \mu M$ were considered.
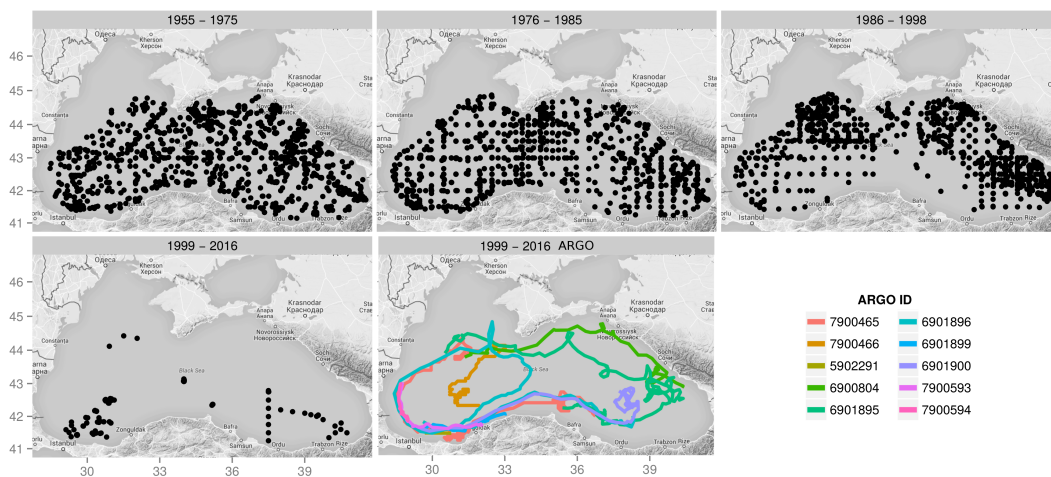
Figure 3. Distribution of the ship-based oxygen profiles (Fig. 2) available for each period (black dots). The last panel displays the trajectories of the ARGO floats. Number of profiles for each period are given in the text. Map data: ©Google 2015.
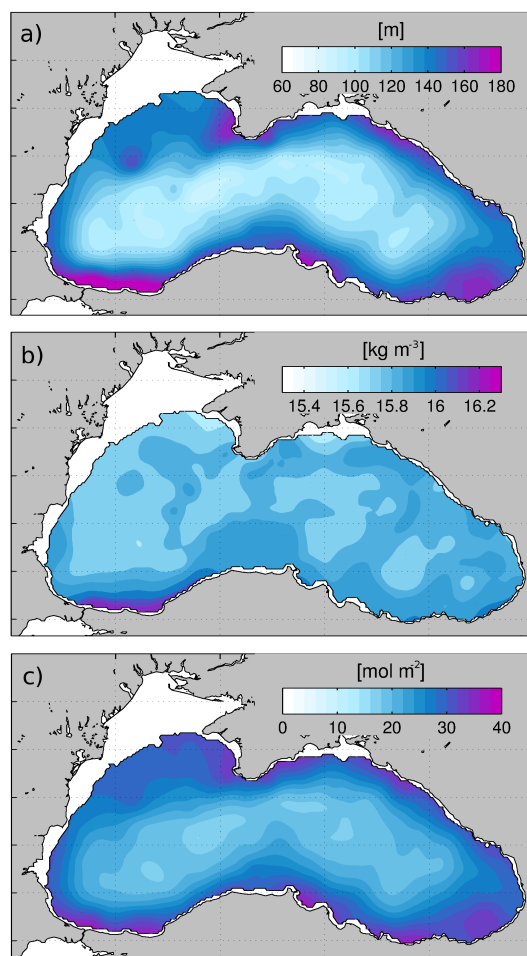
Figure 4. Annual climatologies of **(a)** oxygen penetration depth (where $[O_2] = 20\ \mu$M), **(b)** potential anomaly at oxygen penetration depth and **(c)** oxygen inventory. These spatial climatologies were constructed from the ship-based dataset (1955–2005), accounting for the temporal variability of these diagnostics and the uneven distribution of data (see Sect. 2.3).
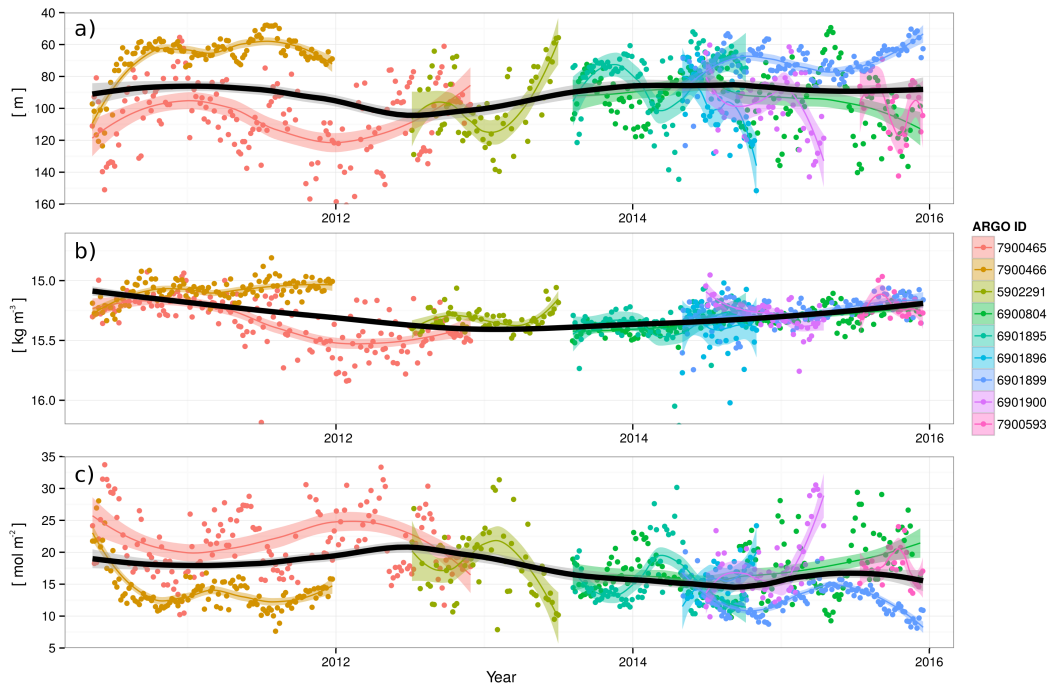
Figure 5. (a) Oxygen penetration depth, (b) Oxygen penetration density levels and (c) oxygen inventory derived from Argo profiles. The color legend gives the unique Argo identification number of the floats. Colored lines and color-filled areas indicate smoothed time series for each float (second degree loess smoother, span=0.5, 0.95 confidence intervals). The black line and gray shaded area are the smoothed time series obtained when considering all floats (reported on Fig. 6).
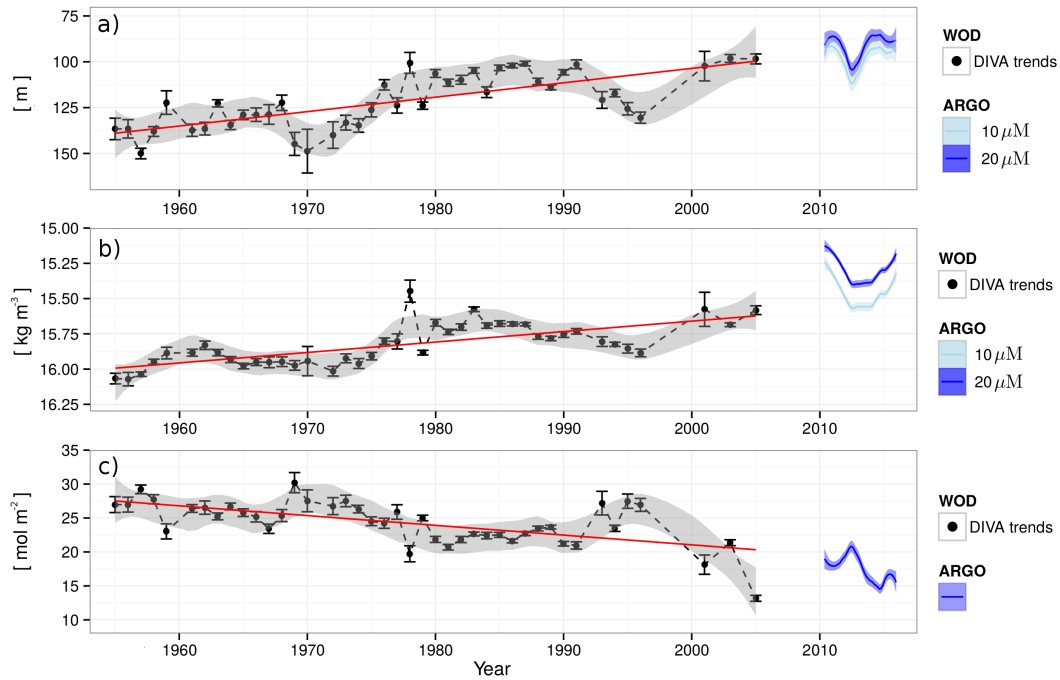
Figure 6. Trends of (a) oxygen penetration depth, (b) oxygen penetration density level (σ_θ) and (c) oxygen inventory deduced from (dots) DIVA analysis of ship-based casts and (blue) ARGO floats. On (a) and (b), the diagnostics from ARGO are also shown for the lower threshold of 10 μM to acknowledge a potential bias between Winkler and Argo data. Red lines: the linear trends assessed from the ship-based data set are -7.9 $\mathrm{m\,decades^{-1}}$, -0.074 $\mathrm{kg\,m^{-3}\,decades^{-1}}$ and -1.44 $\mathrm{mol\,O\,m^{-2}\,decades^{-1}}$ for (a), (b) and (c), respectively. Error bars on DIVA estimated trends indicate the standard error associated with the estimation of the mean misfit for each year (see Appendix A).
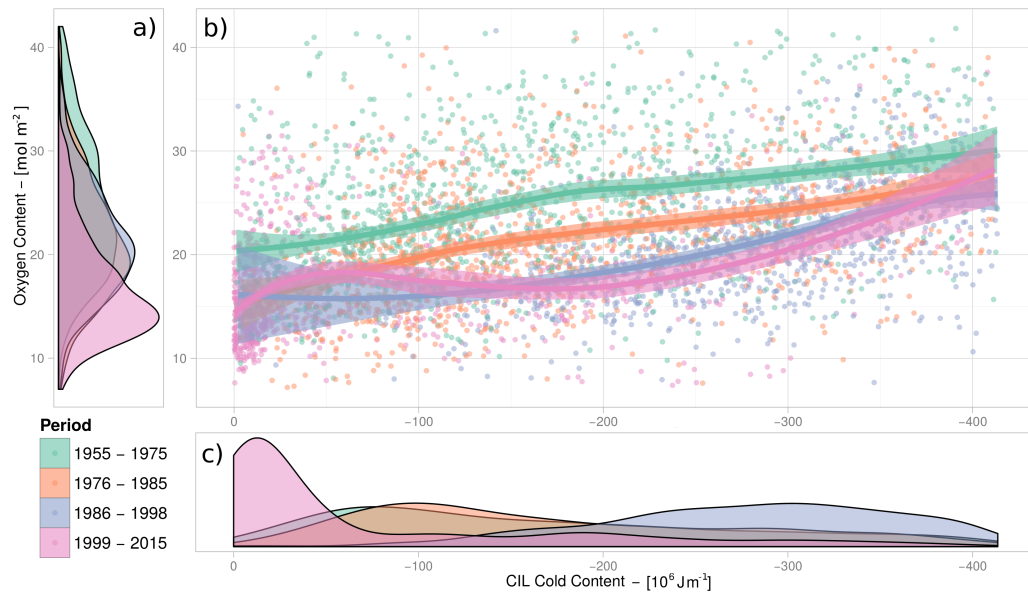
Figure 7. Impact of convective ventilation on oxygen inventory. Frequency distributions of (a) oxygen inventory and (c) Cold Intermediate Layer (CIL) cold content diagnosed from ship-based and Argo profiles for different periods (color legend). (b) Loess regressions (second degree polynomials, span=0.75, Cleveland et al. (1992)) between oxygen inventory and CIL cold content for the different periods (confidence interval $\alpha = 0.99$). The positive relationships observed during each period illustrate the ventilating action of CIL formation as a source of oxygen to the intermediate levels. The shift of these relationships towards lower oxygen inventories indicates shift in the oxygen budgets (higher consumption) that are independent of the intensity of CIL formation.